Bioactive Materials 19 (2023) 487–498

Contents lists available at ScienceDirect

Bioactive Materials

journal homepage: www.keaipublishing.com/en/journals/bioactive-materials

Nanoengineered hydrogels as 3D biomimetic extracellular matrix with injectable and sustained delivery capability for cartilage regeneration

Penglei Cui [a,d,1], Panpan Pan [b,1], Ling Qin [c], Xinluan Wang [c], Xiaodong Chen [a], Yonghui Deng [b,*], Xiaoling Zhang [a,**]

[a] Department of Orthopedic Surgery, Xin Hua Hospital Affiliated to Shanghai Jiao Tong University School of Medicine, Shanghai, 200092, People's Republic of China
[b] Department of Chemistry, Fudan University, Shanghai, 200433, People's Republic of China
[c] Translational Medicine R&D Center, Institute of Biomedical and Health Engineering, Shenzhen Institutes of Advanced Technology, Chinese Academy of Sciences, Shenzhen, 518057, People's Republic of China
[d] Department of Spine Surgery, Beijing Jishuitan Hospital, Peking University Fourth School of Clinical Medicine, Beijing, 100035, People's Republic of China

ARTICLE INFO

Keywords:
Injectable nanocomposite
Mesoporous silica
3D biomimetic extracellular matrix
Sustained release of anhydroicaritin
Cartilage regeneration

ABSTRACT

The regeneration of articular cartilage remains a great challenge due to the difficulty in effectively enhancing spontaneous healing. Recently, the combination of implanted stem cells, suitable biomaterials and bioactive molecules has attracted attention for tissue regeneration. In this study, a novel injectable nanocomposite was rationally designed as a sustained release platform for enhanced cartilage regeneration through integration of a chitosan-based hydrogel, articular cartilage stem cells (ACSCs) and mesoporous SiO_2 nanoparticles loaded with anhydroicaritin (AHI). The biocompatible engineered nanocomposite acting as a novel 3D biomimetic extracellular matrix exhibited a remarkable sustained release effect due to the synergistic regulation of the organic hydrogel framework and mesopore channels of inorganic $mSiO_2$ nanoparticles ($mSiO_2$ NPs). Histological assessment and biomechanical tests showed that the nanocomposites exhibited superior performance in inducing ACSCs proliferation and differentiation *in vitro* and promoting extracellular matrix (ECM) production and cartilage regeneration *in vivo*. Such a novel multifunctional biocompatible platform was demonstrated to significantly enhance cartilage regeneration based on the sustained release of AHI, an efficient bioactive natural small molecule for ACSCs chondrogenesis, within the hybrid matrix of hydrogel and $mSiO_2$ NPs. Hence, the injectable nanocomposite holds great promise for use as a 3D biomimetic extracellular matrix for tissue regeneration in clinical diagnostics.

1. Introduction

Articular cartilage defects are one of the most common orthopedic disease and cause knee joint dysfunction, significant pain and disability, thus leading to heavy economic burdens on the individual patient and society [1,2]. Unfortunately, articular cartilage regeneration remains a considerable challenge because it does not present an instinctive self-healing capacity due to its avascular and aneural nature [3,4]. Tissue engineering is regarded as a promising method for cartilage repair by integrating ideal seed cells [5], suitable biomaterials [6] and biological stimuli [7–10]. Extracellular matrix (ECM) is mainly composed of macromolecular substances (e.g., polysaccharides, proteins) secreted by cells, which possesses an intricate and complex network to support and connect tissue structure. Cells receive signals from the ECM, the natural extracellular microenvironment, regulates biological synthesis and cellular physiological function such as proliferation, apoptosis, migration and differentiation [11]. In recent years, self-healing polymer hydrogels have been demonstrated as promising tissue engineering materials because of their superior biocompatibility, hydrophilicity, low toxicity, injectable [12,13], rapid self-healing and boundary-lubricated capabilities [14–17]. Notably, polysaccharide-based natural marine biomaterials (e.g., chitosan, sodium alginate, chitin) have attracted

Peer review under responsibility of KeAi Communications Co., Ltd.
* Corresponding author.
** Corresponding author.
E-mail addresses: yhdeng@fudan.edu.cn (Y. Deng), xlzhang@shsmu.edu.cn (X. Zhang).
[1] These authors contributed equally to this work.

https://doi.org/10.1016/j.bioactmat.2022.03.032
Received 26 November 2021; Received in revised form 16 March 2022; Accepted 17 March 2022

tremendous attention in tissue mimics *via* providing robust platforms for culturing cells in three dimensions [18], owing to their merits of unique physicochemical properties, 3D network framework and rich marine biological resources [19]. Zhang et al. reported a self-healing antibacterial OSA-COS-ZnO composite hydrogel for skin tissue regeneration, which was fabricated by reversible Schiff base linkages between the $–NH_2$ of chitosan oligosaccharide (COS) and the –CH=O of oxidized sodium alginate (OSA) mixed with zinc oxide nanoparticles (ZnO) [20]. Recent, our group constructed a biocompatible GCS-OSA-CaP hybrid hydrogel for bone regeneration by spontaneous Schiff base reaction formed between the –CH=O of OSA and the $–NH_2$ of glycol chitosan (GCS) mixed with calcium phosphate (CaP) nanoparticles [21]. Benefiting from the unique dynamic equilibrium of the imine in hydrogel networks, these hydrogels exhibit excellent performance in pH-response, injectable and self-healing ability under physiological conditions without any external stimuli. Despite the above-mentioned advantages, the reported hydrogels still have much room for improvement in controlled release of cargo. Tailored mesoporous inorganic biomaterials have been widely utilized for cargo delivery engineering in the field of biomedicine applications [22–28] because of their unique features, including nanoscale size, high specific surface area, controllable mesoscopic structure and physicochemical properties [29,30]. Moreover, multiple biocompatible and degradable nanoparticles (e.g., bioactive glass nanoparticles [31], mesoporous silica microrods [32], hydroxyapatite nanovehicles [33]) have been demonstrated to be effective for bone-related tissue regeneration by virtue of providing functional mineral components of tissue and precisely regulating sustained drug delivery [34–36]. Especially, except for the superoir features of mesoporous nanopartiles, mesoporous silica nanopartiles ($mSiO_2$ NPs) could also provide silicon source for inducing bone mineralization, promoting osteogenesis and angiogenesis [37]. Benefiting from this, Regí's group reported an ALN functionalized PEG-modified $mSiO_2$ nanovehicle acted as biomolecular sustained-release system, which can transport and deliver effectively Sost siRNA and osteostatin by subcutaneous injection to target bone tissue [38]. In particular, the innovative structural and functional combination of self-healing organic polymeric hydrogels with inorganic nanoparticles enables biomimetic composite hydrogels for drug delivery [39,40], regenerative medicine [41–43] and biosensing [44] due to their multiresponsive actuating property [45] and mechanical anisotropy [46–49]. Notably, by combining the diverse merits of bioactive herbal drug small molecules and therapeutic cells to promote chondrogenic differentiation, the preparation of bioinspired injectable composite hydrogels as three-dimensional (3D) biomimetic extracellular matrices has gradually developed into a new research hotspot in the field of cartilage regeneration [50,51]. Great efforts are still needed to optimize herbal drug small molecules and therapeutic cells to promote chondrogenic regeneration.

Cartilage tissue engineering has emerged as a prospective method of regenerating cartilage *in situ*, and hydrogels play a significant role because of their advantageous features, such as flexible mechanical properties and good biocompatibility [52–56]. Bone marrow derived mesenchymal stem cells (BM-MSCs) are regarded as a promising implantable cell source for cartilage regeneration [57] because of their high self-renewal capacity and chondrogenic potential *in vitro* [58,59]. However, cartilage tissues formed through BM-MSCs differentiation are mostly subject to hypertrophy and have difficulty maintaining the cartilage phenotype *in vivo* [60–62], which leads to inferior cartilage regeneration [63]. Recently, articular cartilage has been demonstrated to contain a population of cells with progenitor-like qualities including the ability of self-renewal, the expression of stem cell-related surface markers, and the potential for multilineage differentiation [64,65], and these cells were identified as articular cartilage stem cells (ACSCs) [66–72]. ACSCs play a pivotal role in cartilage development, maturation, repair upon osteoarthritis and response to injury [64,73,74]. Importantly, our previous study found that the chondrogenic ability of ACSCs was higher than that of BM-MSCs, suggesting that ACSCs obtained from articular cartilage exhibit a high degree of chondrogenic characteristics and hold a great promise for use as an ideal cell source and/or drug target for cartilage regeneration [65].

Natural small molecules are regarded as promising drug resources since they possess a wide range of pharmacophores and a high degree of stereochemistry [75,76]. Thus, it is of great significance to explore safe and low-cost bioactive natural small molecules to function as a substitute for or cooperate with growth factors such as transforming growth factor (TGF)-β and insulin-like growth factor (IGF) for cartilage regeneration. Xian-Ling-Gu-Bao capsule (XLGB), the only anti-osteoporosis traditional Chinese medicine prescription (TCMP) listed in the China National Basic Drugs Catalog [77], has been widely used to treat osteoporosis [78]. However, it remains unclear whether the components of XLGB are effective for cartilage regeneration. Anhydroicaritin (AHI), a prenylated flavonoid naturally occurring in several Epimedium species (Berberidaceae family), is commonly recognized as one of the effective compounds of Epimedii Herba, a famous traditional Chinese herbal medicine. Anhydroicaritin exhibits a variety of biological activities, such as insulin resistance and diabetic osteoporosis [79,80]. In this research, a series of experiments was carried out to clarify this hypothesis and the results from multiple perspectives clearly showed that anhydroicaritin, an herbal drug small molecule, can significantly promote chondrogenic differentiation of ACSCs *in vitro*. The maintenance of the proper level of bioactive molecules in the defect site is of utmost importance for the continuous induction of stem cell chondrogenic differentiation and cartilage regeneration. Therefore, it is of great interest to develop a novel cartilage regeneration system to achieve efficient and persistent cartilage regeneration *in situ* by combining ideal stem cells and safe and low-cost bioactive molecules with suitable biomaterials.

Herein, a novel bioinspired injectable composite platform was designed *via* the integration of biocompatible chitosan-based hydrogels, ACSCs and $mSiO_2$ NPs loaded with AHI for utilization as a 3D biomimetic extracellular matrix for dual-continuous payload release and chondrogenic regeneration. The composite hydrogel exhibited remarkable sustained release effect due to the synergistic regulation of the organic hydrogel framework and mesopore channels of inorganic $mSiO_2$ NPs. Histological assessment and biomechanical tests demonstrated that the composite hydrogels exhibited superior performance in inducing ACSCs proliferation and differentiation *in vitro* and promoting extracellular matrix (ECM) production and cartilage regeneration *in vivo*. Furthermore, the composite scaffold was verified to significantly enhance cartilage regeneration based on the sustained release of AHI, which is a novel bioactive herbal small molecule for ACSCs chondrogenesis, within the hybrid matrix and 3D network structure of hydrogels and $mSiO_2$ NPs. These bioinspired and injectable composite hydrogels may provide facile and efficient platforms for tissue regeneration in clinical diagnostics.

2. Results and discussion

2.1. Chondrogenic potential of ACSCs treated with AHI in vitro

Thirteen small molecule compounds were obtained from XLGB according to our previous report [77]. To study the chondrogenic potential of these compounds, the mRNA expression of cartilage-specific genes was examined after incubation with the agents described above. AHI AHI was chosen as the final target for further study because it significantly promotes the mRNA expression of col II (col2a1), aggrecan (acan) and sox9 (Figure S1). Then, to explore the effective and safe concentration of AHI, the proliferation of ACSCs treated with a series of concentrations of AHI in culture was determined *via* a cell counting kit-8 (CCK-8) assay. AHI had almost no effect on the proliferation of ACSCs when the concentration of AHI was equal to or less than 3 μM but significantly decreased the proliferation of ACSCs compared with that at 0 μM when it was greater than 3 μM (Fig. 1a). The results showed that an AHI concentration of 3 μM was the optimal choice and could be used

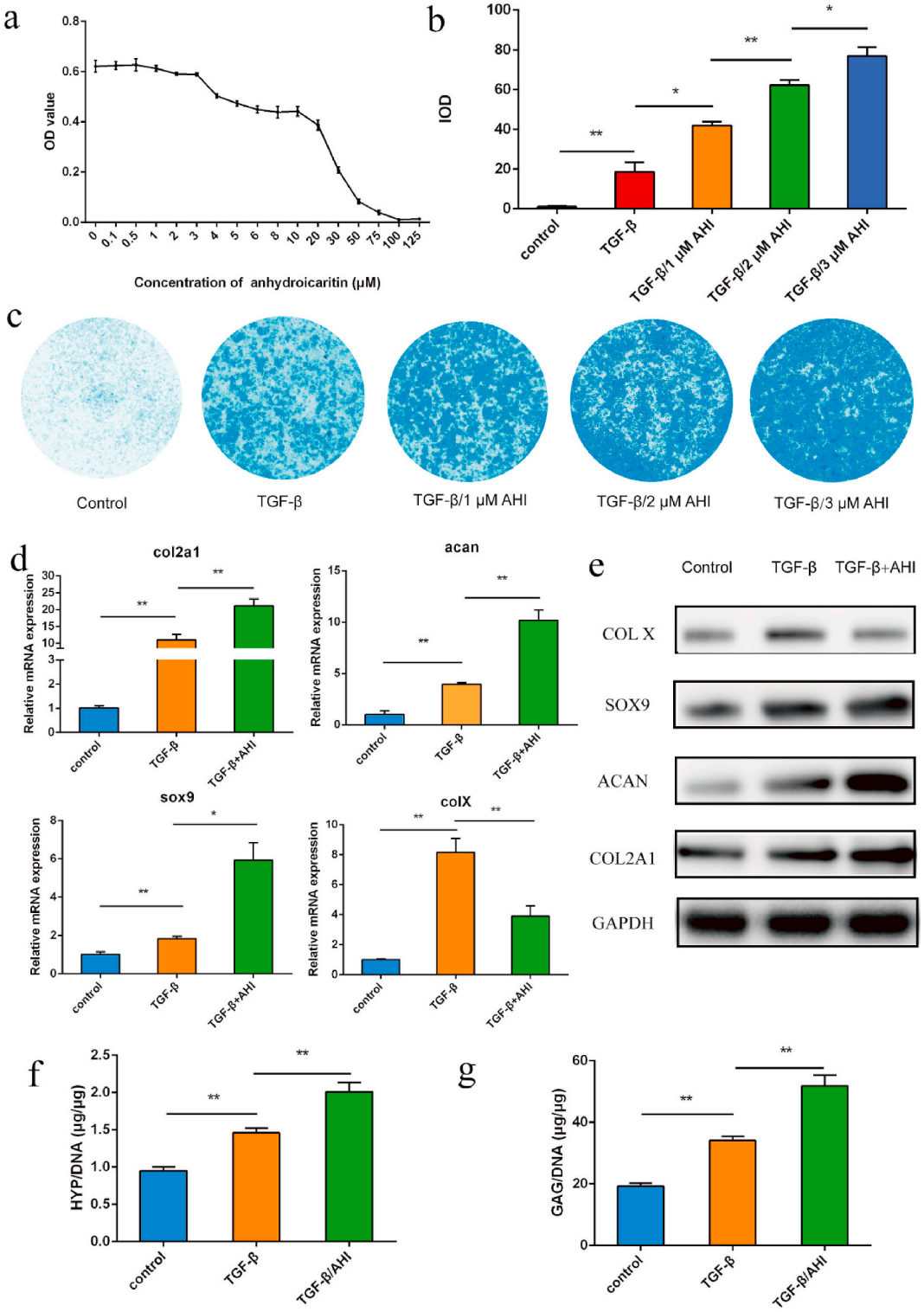

Fig. 1. Chondrogenic potential of ACSCs treated with AHI *in vitro*. a) Effect of AHI on the proliferation of rabbit ACSCs *in vitro*. ACSCs were cultured with various concentrations of AHI (0.1 μM-125 μM) for 3 days. Cell proliferation was determined *via* CCK8 assays. b) Quantitative analysis of alcian blue staining. c) Detection of proteoglycan accumulation in different groups by cytochemical analysis through Alcian blue staining. d) mRNA expression of the cartilage-specific genes, col2a1, acan, and sox9 in the control and experimental groups based on Q-PCR. e) Protein expression of col2a1 by Western blot. f) Quantification of collagen production in different groups via the HYP assay. g) Quantification of the production of cartilaginous matrix in different groups by the GAG assay (n = 3, *p < 0.05, **p < 0.01).

without affecting the proliferation of ACSCs. To further study the potential of AHI on the chondrogenic differentiation of ACSCs, the expression of cartilage-specific genes was examined by Q-PCR and Western blot. Alcian blue staining was used to detect proteoglycan accumulation 21 days after the chondrogenic differentiation of ACSCs, and the staining intensity was quantified by ImageJ software. The TGF-β/AHI groups displayed higher staining intensity than the TGF-β group (Fig. 1b, c, **S3**b). The mRNA expression levels of cartilage-specific genes, collagen II (col2a1), aggrecan (acan) and sox9, significantly increased (Fig. 1d), and the protein expression levels of collagen X (COL

X), COL2A1, SOX9 and ACAN were also remarkably enhanced (Fig. 1e) in ACSCs treated with TGF-β/AHI compared with those with TGF-β treatment. The mRNA expression levels of COL X significantly decreased (Fig. 1d), and the protein expression levels of collagen X was reduced in in ACSCs treated with TGF-β/AHI compared with those without TGF-β treatment. Consistent with the mRNA expression of cartilage-specific genes, ACSCs treated with TGF-β/AHI showed greater chondrogenic capacity than ACSCs treated with TGF-β, as evidenced by higher hydroxyprolin (HYP) and glycosaminoglycan (GAG) contents *in vitro* (Fig. 1f and g). Therefore, it can be concluded that AHI can significantly promote chondrogenic differentiation of ACSCs and inhibit chondrocyte hypertrophic differentiation *in vitro*.

2.2. Physicochemical properties of the bioinspired composite hydrogel

Herein, a novel bioinspired and biocompatible composite platform was developed to achieve efficient and persistent cartilage regeneration *in situ*, and it combines injectable hydrogels with ACSCs and AHI-loaded $mSiO_2$ NPs (denoted as AHI-$mSiO_2$ NPs) (Scheme 1). $mSiO_2$ NPs that act as a reservoir and carrier for AHI by utilization of their high porosity were employed to regulate the continuous release of AHI. First, the AHI-$mSiO_2$ NPs and glycol chitosan (GCS) were dispersed and dissolved in PBS (pH 7.4) to form a homogeneous suspension solution. Then, oxidized sodium alginate (OSA) was added to the suspension solution, resulting in GCS-OSA-AHI-$mSiO_2$ composite hydrogel (denoted as GOAS) through a short-lived self-healing process. In particular, when OSA and ACSCs were added together into the suspension solution, the precursor of the GCS-OSA-AHI-$mSiO_2$-ACSCs composite hydrogel (denoted as GOAS-ACSCs) was obtained. Subsequently, the GOAS-ACSCs composite hydrogel precursor was immediately injected into the cartilage defect to form a dense composite hydrogel *in situ via* a Schiff base reaction at 37 °C without external stimulation, such as by chemical crosslinkers or UV, throughout the fabrication process.

The GOAS composite hydrogel was obtained by condensation reaction of the –CHO group from OSA with the –NH_2 group from GCS during mixing together with AHI-$mSiO_2$ NPs, leading to rich dynamic –CH=N– groups in the hybrids [81]. After the reaction, new peaks at approximately 1630 cm^{-1} were found for the obtained GOAS composite hydrogel, and the characteristic absorption bands of GCS (–NH_2 groups) and OSA (CH=O groups) disappeared [82], indicating the formation of –CH=N– bonds through the Schiff base reaction. Moreover, the characteristic peaks of AHI were preserved in the obtained GOAS composite hydrogel, implying that the AHI was stable throughout the hydrogel preparation process (Figure S5 e) [83,84].

Without special requirements regarding environmental conditions and equipment, whole gelation fabrication can be readily accomplished using the sample 60 s vortex process at 37 °C (Fig. 2a). The $mSiO_2$ NPs obtained *via* a surfactant mediated *sol-gel* reaction [85] have a uniform diameter of ~178 nm and smooth surface (Figure S6 a, b), and they can be homogeneously dispersed in aqueous solution because of their hydrophilic surface with rich silanol groups. Numerous radially aligned mesopores are clearly visible in the $mSiO_2$ NPs, indicating high porosity and highly accessible pore channels, which are favorable for the intelligent loading of drugs and sustainable release of guest compounds, such as AHI molecules (Figure S6 c). Nitrogen adsorption-desorption measurements revealed that the $mSiO_2$ NPs have uniform pore size of 2.1 nm, ultrahigh Brunauer-Emmett-Teller (BET) surface area (964 m^2/g), and large pore volume (0.504 cm^3/g) (Figure S8 a, b). AHI molecules were loaded into the $mSiO_2$ NPs through a nanocasting method by impregnating of $mSiO_2$ NPs in a PBS solution of AHI followed by solvent evaporation. The *in vitro* drug release behavior of the composite material was examined, as shown in Fig. 2b. The hydrogel (donated as GOA) and AHI-$mSiO_2$ NPs exhibited a sudden release at the beginning of two weeks and then a gradually slowing release of AHI, with a cumulative release of 91.0 ± 4.33% and 87.52 ± 2.97%, respectively. Sudden release occurred in the first two weeks due to the fast diffusion of AHI located at the region near the surface of carriers. However, the GOAS composite hydrogel demonstrated a significant sustained slow drug

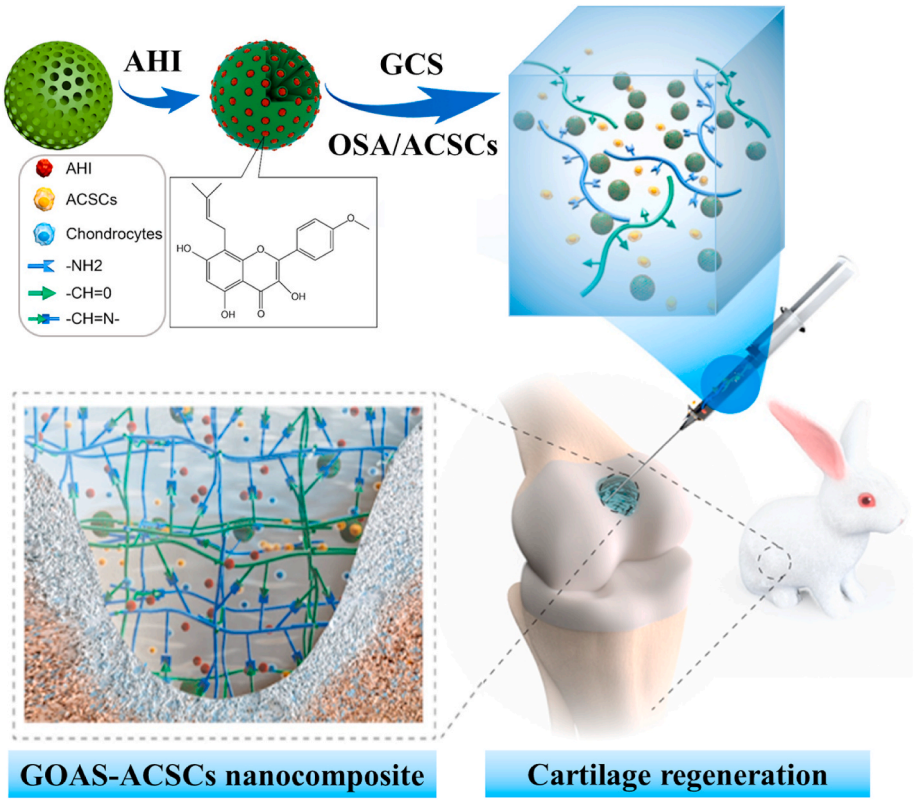

Scheme 1. Illustration of the fabrication and cartilage regeneration application of the injectable GOAS-ACSCs engineered nanocomposite.

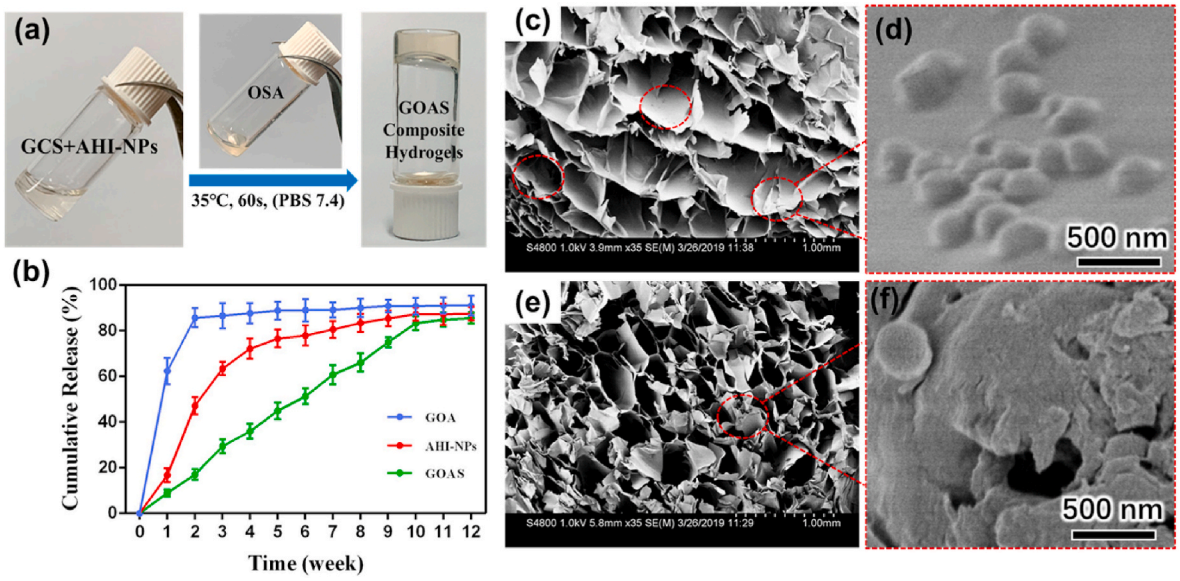

Fig. 2. a) Photographs demonstrating the formation of between the aqueous suspension of AHI-loaded $mSiO_2$ and GCS and the OSA solution for 60 s in PBS (pH 7.4). b) Drug release curves of GOA hydrogels, AHI-loaded $mSiO_2$NPs, and GOAS composite hydrogels. SEM images (c–f) of GOAS composite hydrogels after freeze drying viewed from cross-section and e) measuring section of. Scale bar: 1 mm. d) and f) Partial enlargement images of c) and e), respectively. Scale bar: 500 nm.

release for up to 10 weeks, and the cumulative release was 85.58 ± 2.37%. It is worth mentioning that the sustained release behavior was not only attributed to the numerous radially aligned mesoporous channels of $mSiO_2$ NPs but also the 3D network structure of the organic hydrogels. Such unique sustained release behavior indicates its potential for *in vivo* biomedicine applications. After mixing AHI-$mSiO_2$ NPs with OSA and GCS, the obtained GOAS composite hydrogel was freeze-dried for the structure analysis. SEM observations indicated that the dried composites have an open microporous structure and homogeneous distribution of AHI-$mSiO_2$ NPs in cross-section (Fig. 2c). The uniform distribution of AHI-$mSiO_2$ NPs in the hybrid nanocomposite without phase separation is favorable for the sustainable release of AHI by the regulation of mesopore channels and the polymeric hydrogel.

2.3. Nanocomposites enhanced the chondrogenic differentiation of ACSCs in vitro

To test the chondrogenic efficacy of the bioactive sustained release system, ACSCs and AHI-$mSiO_2$ NPs were encapsulated in the hydrogel to establish a 3D culture system *in vitro*. First, live/dead assay and CCK-8 assay demonstrated that almost all ACSCs encapsulated in the platform were stained green and the GCS-OSA-$mSiO_2$ NPs composite hydrogel (denoted as GOS) group did not obviously differ from the GOAS group (Fig. 3a). Compared to the control group (cells cultured in dishes), the GOS group and GOAS group had no significant effect on the viability of ACSCs by CCK-8 assay (Fig. 3b). The findings indicated that the bioinspired nanocomposites exhibited excellent biocompatibility for cell survival and proliferation. Then, the chondrogenic potential of ACSCs on the composite hydrogel was detected by analyzing the cartilage-specific gene expression of ACSCs and measuring the content of HYP and GAG in a 3D culture system *in vitro*. Compared to the GOS-ACSCs group, a higher mRNA level of cartilage-specific genes, such as acan, col2a1, and sox9, was observed in the GOAS-ACSCs group after coculture for 7, 14 and 21 days (Fig. 3c). Consistent with the mRNA expression of cartilage-specific genes, the protein level of COL2A1 was higher in the GOAS-ACSCs group (Fig. 3d). In addition, compared with the GOS-ACSCs group, the GOAS-ACSCs group exhibited higher chondrogenic capacity according to the detection of HYP and GAG content (Fig. 3e and f). The above features and performances of the nanocomposite in terms of biocompatibility, sustained release of AHI and enhanced ACSCs chondrogenic differentiation encouraged us to perform further *in vivo* studies.

2.4. Nanocomposites for in vivo cartilage tissue engineering

To evaluate the ability of the nanocomposite to promote cartilage regeneration *in vivo*, cylindrical cartilage defect models (4 mm in diameter, 1.5 mm in depth) were constructed in the center of the trochlear groove in New Zealand white rabbits [86]. The prefabricated precursor of the GOS-ACSCs and GOAS-ACSCs nanocomposite were injected into the cartilage defect site, and the nanocomposites formed *in situ* within 60 s. After 4 weeks, the defects remained empty in the nontreated group (Fig. 4a, d, e). Compared with the nontreated group and GOS-ACSCs, although defects were still observed in GOAS-ACSCs group, partial filling of defects was clearly observed. After 8 weeks, cartilage defects could still be observed in the control group and GOS-ACSCs group; however, the repaired tissue almost fully filled the defects in the GOAS-ACSCs group (Fig. 4a, d). The International Cartilage Repair Society (ICRS) score was designed to assess the integration of the cell-hydrogel construct into the trochlear groove [87]. The ICRS score in the GOAS-ACSCs group was higher than that in the GOS-ACSCs group and 1.9 times higher than that in the nontreated group (Fig. 4e). After 12 weeks, a large cartilage defect was obviously observed in the nontreated group, and a cartilage defect in the central part was still clearly visible in the GOS-ACSCs group. Notably, the GOAS-ACSCs group revealed a smooth and white transparent appearance that was well-integrated with surrounding tissue (Fig. 4a, d). In addition, the ICRS scores of the GOAS-ACSCs group and nontreated group were the highest and lowest, respectively (Fig. 4e). Biomechanical testing of the repaired cartilage was performed at 12 weeks post-implantation. The reduced modulus of the GOAS-ACSCs group was significantly enhanced compared with that of the other two groups (Fig. 4b). In addition, the mean hardness value of the GOAS-ACSCs group was 403 kPa, which closely resembled that of the normal healthy cartilage and was nearly 2 times higher than that of the GOS-ACSCs group and 3.7 times higher than that of the nontreated control group (Fig. 4c). The above results suggest that the injectable GOAS-ACSCs nanocomposite acting as a 3D biomimetic ECM has outstanding performance for functional cartilage regeneration.

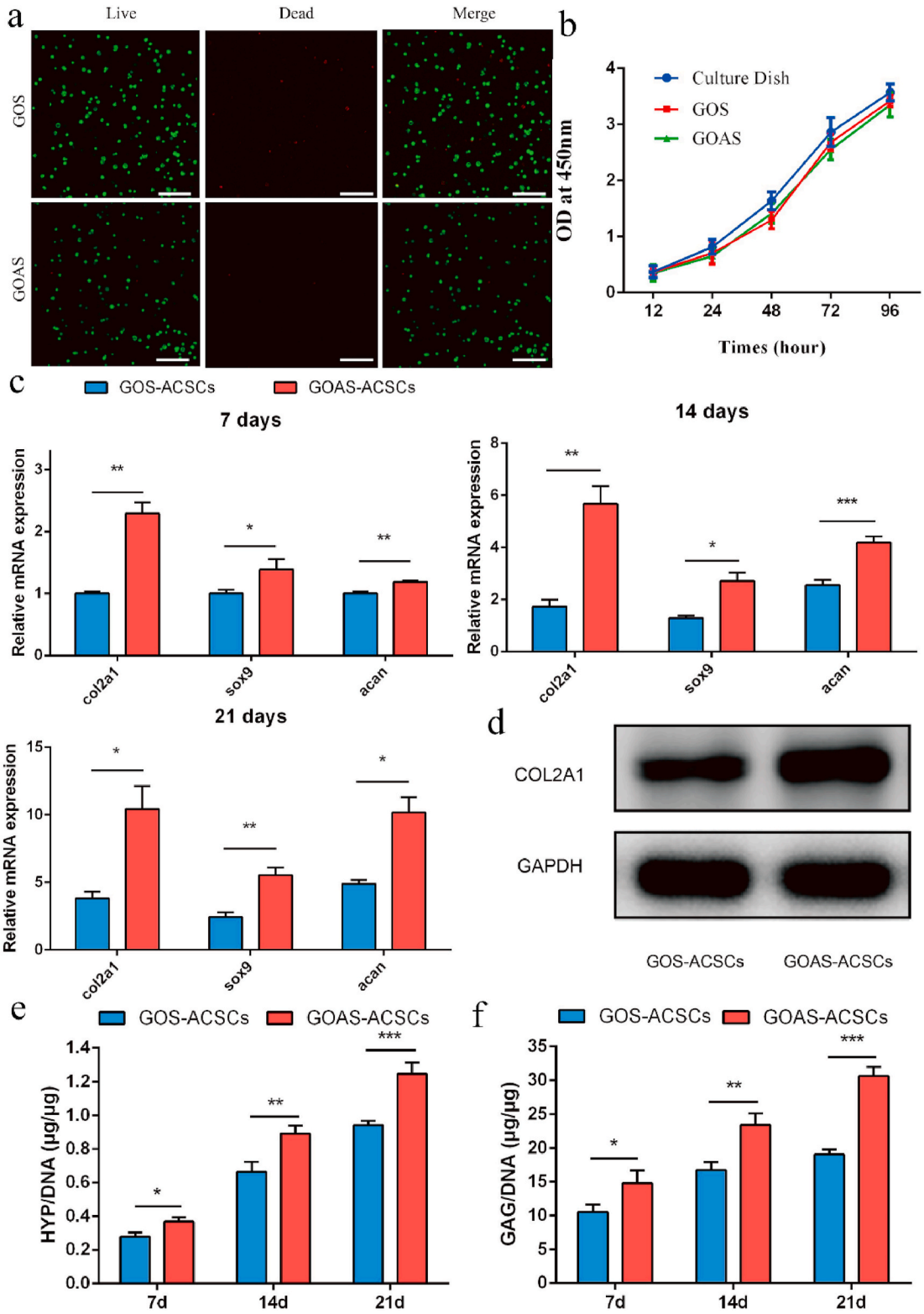

Fig. 3. Chondrogenic potential of ACSCs treated with AHI in 3D culture. a) Live/dead assay of ACSCs encapsulated in different hydrogels on confocal images. (Scale bar = 200 μm) b) Viability of ACSCs encapsulated in experimental and control hydrogels. c) mRNA expression of the cartilage-specific genes, col2a1, sox9, and acan based on Q-PCR. d) The protein expression of cartilage-specific gene col2a1 by Western blot. e) Quantification of the collagen production in different hydrogels by the HYP assay. f) Quantification of cartilaginous matrix production in different hydrogels via the GAG assay (n = 3, *p < 0.05, **p < 0.01, ***p < 0.001).

2.5. Histological assessment of repaired cartilage in vivo

To further evaluate the efficacy of the cell hydrogel on 3D cartilaginous ECM and collagen type II synthesis, toluidine blue staining and collagen II immunohistochemistry of neocartilage were performed. At 4 weeks, the defect site was partially filled with some regenerated tissue and almost empty in the nontreated group (Figs. 4d and 5a). In the GOAS-ACSCs group, more hyaline cartilage-like ECM was observed in

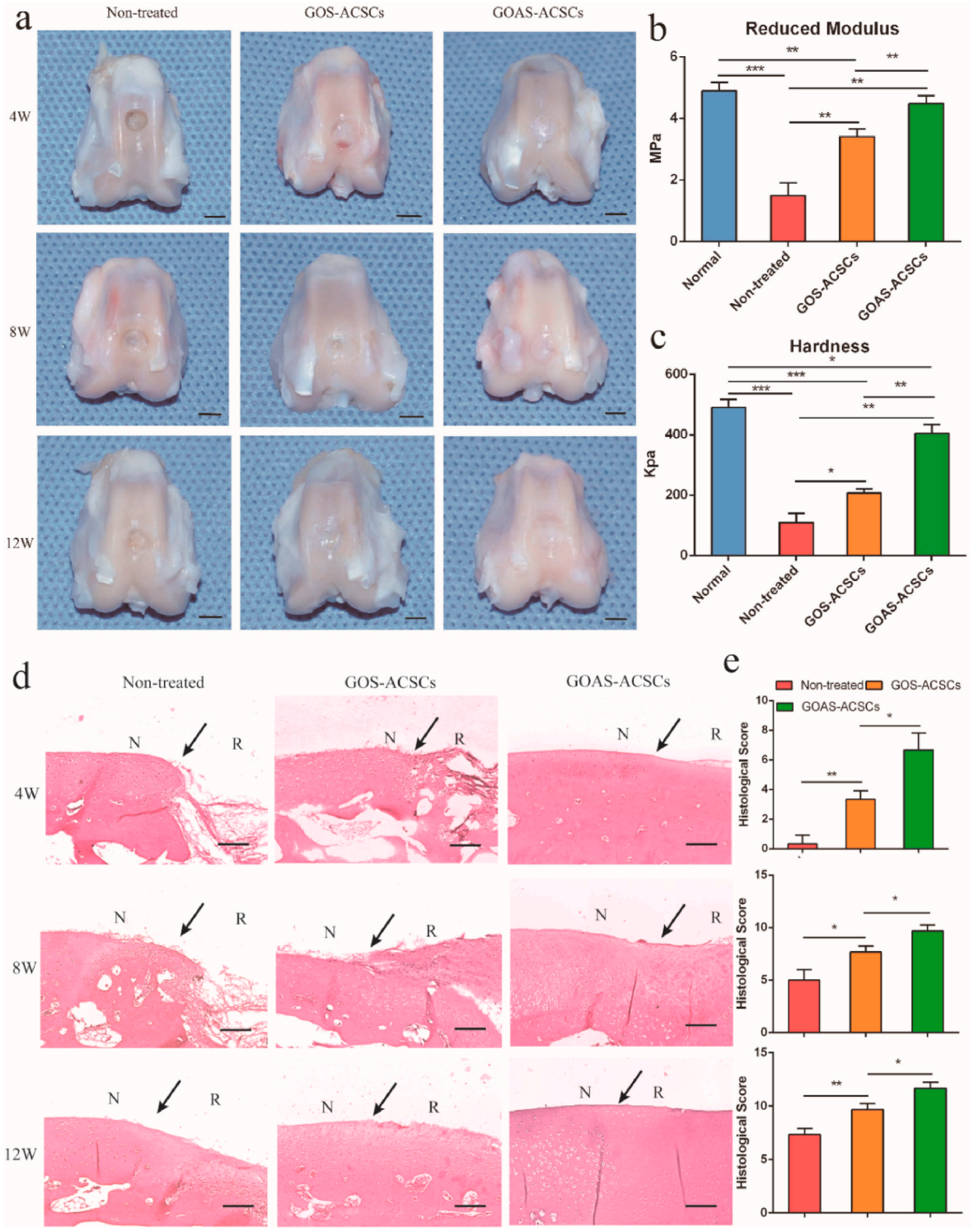

Fig. 4. Macroscopic observation, histological scoring and biomechanical tests of repaired cartilage *in vivo*. a) Macroscopic appearance of the specimens harvested at 4, 8 and 12 weeks after surgery. Biomechanical properties of repaired cartilage in different groups: b) reduced modulus and c) hardness. (n = 3, *p < 0.05, **p < 0.01, ***p < 0.001, scale bar = 5 mm) d) H&E staining of repaired cartilage at 4, 8, and 12 weeks (N: native cartilage; R: repaired cartilage; the arrow indicates the edge of native cartilage and repaired cartilage). e) Histological score for repaired cartilage at 4, 8, and 12 weeks. (n = 3, *p < 0.05, **p < 0.01, scale bar = 200 μm).

the cartilage defects than in the GOS-ACSCs group. At 8 weeks, the defects were filled with a few regenerated tissues and nearly no neocartilage was observed in the nontreated group. In the GOAS-ACSCs group, large amounts of hyaline cartilage-like ECM were observed in the cartilage defects (Fig. 5a and b). At 12 weeks, the defects were filled with more regenerated tissues in the nontreated group (Figs. 4d and 5a). The defects were filled with a mixture of hyaline cartilage-like tissue, and obvious clefts were observed in the GOS-ACSCs group (Fig. 5a and b). It is worth noting that the GOAS-ACSCs group exhibited good interaction between the regenerated tissue and surrounding normal cartilage, and

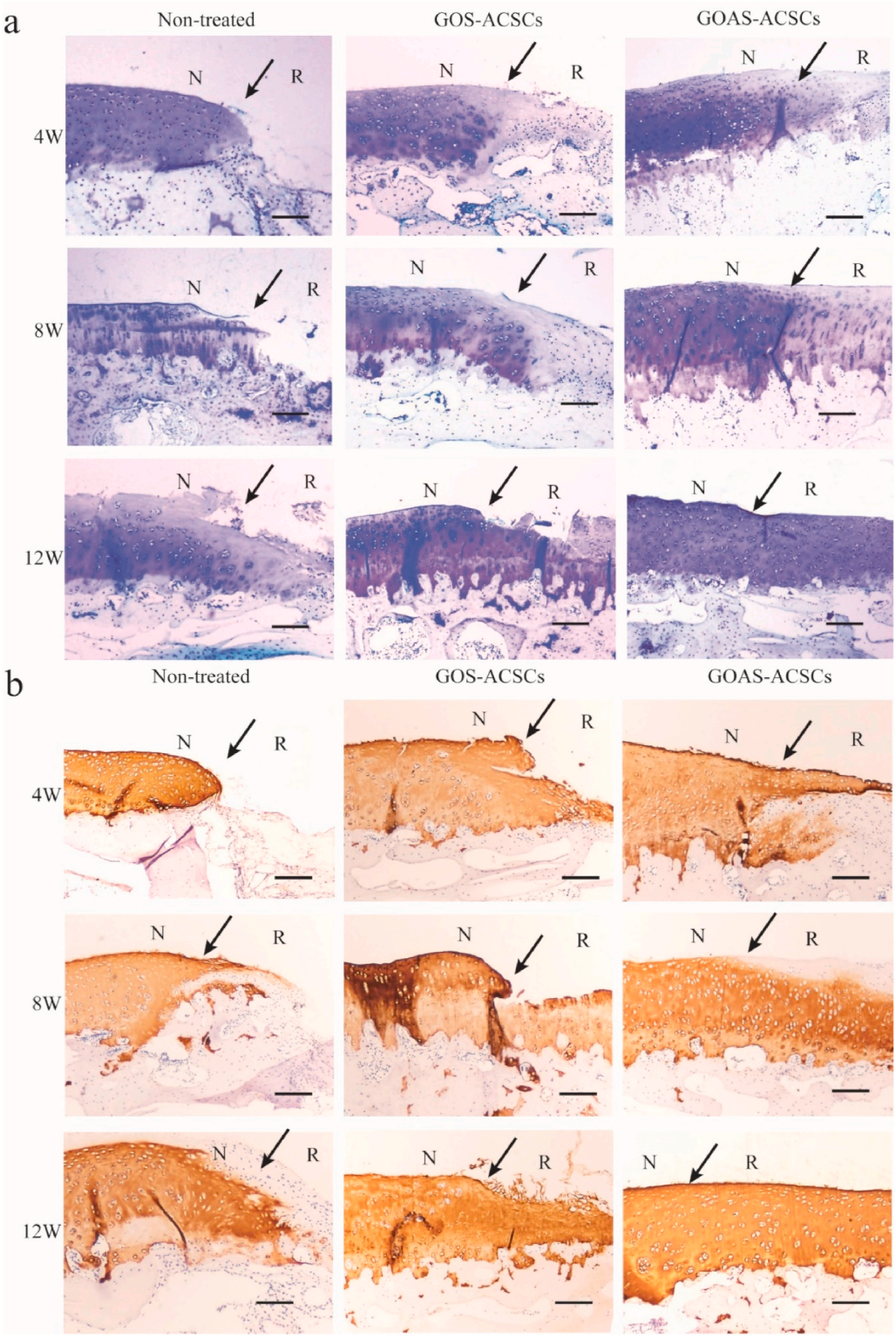

Fig. 5. Histological assessment of repaired cartilage *in vivo*. a) Toluidine blue staining of repaired cartilage at 4, 8, and 12 weeks. (N: native cartilage; R: repaired cartilage; the arrow indicates the edge of native cartilage and repaired cartilage). b) Immunohistochemical staining for collagen type II at 4, 8, and 12 weeks (n = 5, scale bar = 200 μm). Bioinspired injectable engineered nanocomposites acting as a 3D biomimetic extracellular matrix were demonstrated to significantly enhance cartilage regeneration based on the sustained release of AHI loaded into the mesoporous channel of $mSiO_2$ NPs and *in situ* injection of a hybrid cell-hydrogel matrix. This integration strategy for mulfunctional nanocomposites may serve as a potential pathway for optimizing the local microenvironment of defect sites and inducing transplanted and endogenous stem cells to participate in tissue regeneration.

toluidine blue and collagen II staining showed the largest amount of hyaline cartilaginous tissues, thus indicating that neotissue almost fully filled the defects, which were flush with the native tissue. Overall, the engineered cell-hydrogel nanocomposite was a prospective platform for 3D cartilaginous biomimetic ECM synthesis and cartilage regeneration by providing ACSCs and releasing the chondro-inductive natural molecule AHI.

Herein, we constructed ACSCs-laden chitosan-based hydrogel mixed with AHI-encapsulated $mSiO_2$ NPs to stimulate cell behavior to further induce more biomimetic tissues. Moreover, the development of composite hydrogel with 3D network framework that can imitate tissue microenvironment and the physiological biomineralization process shows important therapeutic significance for articular cartilage regeneration [88]. The physiochemical properties of the injectable cell-hydrogel engineering nanocomposite are similar to those of native extracellular matrix, which can be employed as a cargo transport system

for cartilage tissue regeneration. In order to achieve the rapid development of multi-mechanisms, multifunctional self-healing hydrogels and promote the effective expansion of its application in biomaterials and intelligent soft materials, the future research direction of self-healing hydrogels mainly focused on some aspects: the design of self-healing hydrogels that can self-heal in a variety of environments, design of self-healing hydrogels combined with dynamic covalent/non-covalent interactions, self-healing hydrogel for flexible electronic devices and so on.

3. Conclusion

In summary, the herbal small molecule AHI was identified as a bioactive factor for promoting chondrogenic differentiation of ACSCs. Furthermore, the injectable cell-hydrogel engineering nanocomposite was rationally designed to achieve sustained AHI release and one-step cartilage regeneration *in situ* by integrating OSA with AHI-mSiO_2 NPs composited GCS and ACSCs. The sustained release behavior of AHI was ascribed to the synergistic effect of mesopore channels of inorganic mSiO_2 NPs and the 3D organic hydrogel framework. The biocompatible multifunctional composite hydrogel system exhibited superior advantages for inducing ACSCs proliferation and differentiation *in vitro*, promoting 3D ECM production and cartilage regeneration *in vivo*, because of its dual merits in *in situ* injection and fast self-healing of 3D viable cell-hydrogels and sustained release of bioactive factors for a long-lasting effect. Considering the simplicity and high efficiency, this integration strategy for the construction of functionally engineered nanocomposites may also serve as a potential pathway for optimizing the local microenvironment of defect sites and inducing stems cells to participate in tissue and organ regeneration.

4. Experimental section

Chemicals: Tetraethyl orthosilicate (TEOS), ethanol, sodium alginate (SA>350 MPa s), concentrated ammonia solution (28 wt%), $NaIO_4$ and anhydroicaritin (AHI, purity ≥99%) were all of analytical grade (Shanghai Chemical Corp.). Glycol chitosan (GCS, polymerization degree 400, assay 60%), cetyltrimethylammonium bromide (CTAB) and alcian blue were supplied by Aldrich-Sigma. Trypsin-EDTA (0.25%) was obtained from Invitrogen. Dulbecco's modified Eagle's medium (DMEM)/F-12 1:1 and phosphate buffered saline (PBS) were supplied by HyClone. Fetal bovine serum (FBS) was purchased from Gibco. Cell Counting Kit-8 (CCK-8) was obtained from Dojindo Molecular Technology. All other chemicals were utilized as received. Deionized water was utilized for all experiments.

Cell isolation, culture and chondrogenic differentiaiton: ACSCs were isolated using fibronectin through an *in vitro* adhesion assay according to previous report [65]. In brief, knee articular cartilage of rabbits (12 weeks old) was sliced and then cut into small slices. Subsequently, the trypsin-EDTA (0.25%, Invitrogen) was used to digest small slices for 10 min. DMEM/F-12 1:1 containing 10% FBS was added to stop the trypsin-EDTA digestion. The slices were washed with sterile PBS and digested in collagenase type II (0.02 wt/vol%) for 5 h. Fibronectin (10 μg/ml) was added to six-well plates. After 12 h, the isolated cells were seeded into six-well plates coated with fibronectin in complete DMEM/F-12 1:1 medium. After 20 min, the medium was removed and the cells adhering to the bottom of the six-well plates were ACSCs. The ACSCs were cultured under static conditions in a humidified, 37 °C incubator with 95% air and 5% carbon dioxide. ACSCs were incubated in chondrogenic induction medium for 28 days (1% vol/vol insulin-transferrin-sodium selenite, 10^{-7} M dexamethasone, 1 mM sodium pyruvate, 50 mM ascorbate-2-phosphate, 50 mg/mL proline, and 20 ng/mL transforming growth factor-β).

Trilineage differentiation of ACSCs: In brief, ACSCs of passage 3 were harvested and incubated in chondrogenic induction medium for 21 days (1% vol/vol insulin-transferrin-sodium selenite, 10^{-7} M dexamethasone, 1 mM sodium pyruvate, 50 mM ascorbate-2-phosphate, 50 mg/mL proline, and 20 ng/mL transforming growth factor-β3), adipogenic induction medium for 14 days (1 mM isobutylmethylxanthine and 10^{-3} mM dexamethasone), and osteogenic induction medium (10 mM glycerol-2-phosphate, 0.1 mM dexamethasone, and 20 mM ascorbic acid) for 14 days. The cells were incubated at 37 °C in an atmosphere with 5% CO_2. Alizarin red staining (day 14) was performed to detect osteogenesis, and Oil-Red-O staining (day 14) was performed to assess the adipogenic potency. After 21 days of chondroinduction, Alcian blue staining was conducted to evaluate chondrogenesis.

Cytotoxicity assay: The cytotoxicity assay was performed using a standard protocol [89]. In brief, ACSCs were digested in 0.25% trypsin-EDTA when they reached 80–90% confluence. ACSCs were seeded into 96-well plates at 1×10^4 cells/well. After 12 h, fresh medium containing different concentrations of AHI was added to each well. Cells were incubated for 72 h in a humidified atmosphere with 5% CO_2 at 37 °C. Afterwards, the CCK-8 method was used to evaluate the cytotoxicity of AHI. CCK8 was added to each well and the cells were cultured at 37 °C for 2 h. Cell viability was obtained by a microplate reader (Infinite M200 PRO, TECAN, Switzerland).

Alcian blue staining and analysis: The cell layer was washed with PBS, and fixed in 4% polyoxymethylene for 10 min at room temperature. Then the fixed cell layer was immersed in 1% alcian blue dissolved in 3% acetic acid (pH 2.5) at 37 °C. After 30 min, the cell layer was washed with double distilled H_2O. The stained cells were photographed and quantified by ImageJ software (National Institutes of Health).

Quantitative real-time PCR analysis: ACSCs were seeded into six-well plates and complete DMEM/F12 1:1 medium was incubated with the cells. TRIzol reagent (Invitrogen) was used to extract total RNA from ACSCs in accordance with the manufacturer's instructions. Real-time PCR was carried out using the LightCycler 480 system (Roche) and the SYBR Green PCR Kit (Takara) in accordance with the manufacturer's instructions. The data were analyzed to calculate the relative gene expression by the comparison Ct ($2^{-\Delta\Delta}$CT) method. The sequences of the gene primers are listed in Table S1.

Western blot analysis: RIPA lysis buffer (Biocolors, China) was used to obtain total protein content from ACSCs, and the concentration of proteins was determined via the BCA protein assay (Thermo Fisher, United States). Lysate proteins (25 μg) were separated via 10% SDS-PAGE and transferred to nitrocellulose blotting membranes (GE Healthcare Life Science, Germany). Subsequently, 5% bovine serum albumin (BSA) in TBS-Tween (TBS: 0.05 M Tris and 0.15 M NaCl, pH 7.4; 0.2% Tween-20) was used to block the membranes for 60 min. Then the membranes were incubated with primary antibodies (anti-collagen type II, 1:200, #CP18; Calbiochem, Darmstadt, Germany) overnight at 4 °C. All experiments were repeated independently in triplicate.

Sulfated GAG and HYP quantification: The detection of GAG and HYP content was carried out according to a previously reported method [90]. The medium was given to ACSCs and ACSCs-loaded hydrogels. At different time points, the constructs were used for gene analysis and biochemical analyses (ds-DNA, GAG and HYP contents). A Varioskan Flash reader was used to quantify the content of DNA, GAG and HYP. Prepared papain (Sigma) was used to digest the ACSCs and ACSCs-loaded hydrogels at 60 °C overnight for the measurement of ds-DNA and GAG content after weighting with a microbalance. The DNA content was tested against standard curves of calf thymus DNA (Sigma). The total content of sulfated GAG was detected by the dimethylmethylene blue (DMMB, Sigma) assay. The content of GAG was calculated based on the standard curve obtained from chondroitin 6-sulfate from shark (Sigma, USA). The collagen content was quantified by determining the HYP content. The HYP content was examined against a standard curve of L-HYP (Sigma). The GAG and HYP were both normalized by the ds-DNA content.

Preparation of mSiO_2 NPs: The mSiO_2 NPs were synthesized by the *sol-gel* method as previously reported [91]. In a typical synthesis, CTAB (0.54 g) was dispersed in a mixture solution containing 120 mL of

deionized water, 60 mL of ethanol and 3.0 mL of concentrated ammonia solution by ultrasonication. Then, TEOS (0.85 g, 2.21 mmol) was added dropwise into the solution over 1 h. The above-obtained mixture was stirred at 180 rpm/min for 8 h at 25 °C. Finally, the product was collected by centrifugation, and washed with water three times. After drying for 12 h at 40 °C, the sample was calcined for 6 h at 550 °C in air to decompose CTAB template, and then uniform $mSiO_2$ NPs with high porosity were obtained.

Preparation of AHI-encapsulated $mSiO_2$ NPs: Four-hundred milligrams of AHI was dissolved in PBS solution (pH = 7.4, 4.0 mL) under ultrasonication treatment. Then, the above $mSiO_2$ NPs were dispersed in AHI solution with vigorous stirring. After continuous stirring overnight, the resultant solution was allowed to evaporate to remove the solvent and the collected powder sample was rinsed three times by PBS to wash off the unloaded drug. The obtained product was collected for further use.

Preparation of composite hydrogel: Oxidized sodium alginate (OSA, 50% oxidation degree) was prepared according to previously reported methods [92]. As demonstrated in our previous report [21], in order to obtain optimized self-healing capability, the molar ratio of $–NH_2$ bonds from GCS and –CHO bonds from OSA in each composite hydrogel was selected as 0.6. In the synthesis process of the composite hydrogel, 350 μL of the AHI-encapsulated $mSiO_2$ NPs were first dispersed in the GCS PBS solution (6 mL, 3 wt%) under ultrasonication treatment. Then, the OSA PBS solution (1.08 mL, 10 wt%) was rapidly dispersed in the above reaction solution. Shortly after 60 s of vortexing at 35 °C, the reaction mixture was immediately converted into the GCS-OSA hydrogel composited with AHI-encapsulated $mSiO_2$ NPs (denoted as GOAS composite hydrogel). Under the same synthetic conditions, no AHI-encapsulated $mSiO_2$ NPs were added to the GCS PBS solution to form the GCS-OSA hydrogel (denoted as GO hydrogel). Compared with the process of GOAS, same amount of AHI was directly dispersed into the GCS PBS solution without adding of $mSiO_2$ nanocarrier and stirred for 2 h to form the GCS-OSA-AHI hydrogel (denoted as GOA composite hydrogel). Pure $mSiO_2$ NPs without encapsulated AHI were added to the GCS PBS solution to form the GCS-OSA-$mSiO_2$ hydrogel (denoted as GOS composite hydrogel).

Preparation of the ACSCs cocultured engineering nanocomposite: GCS complete DMEM/F12 1:1 medium (83.9 μL, 3 wt%) containing AHI-encapsulated $mSiO_2$ NPs, OSA complete DMEM/F12 1:1 medium (15.1 μL, 10 wt%), and ACSCs (1 μL, 2×10^9/mL) were quickly mixed by vortexing, thus becoming hydrogel precursors. After reacting at 25 °C for 60 s, ACSCs 3D cocultured engineered nanocomposites (denoted as GOAS-ACSCs) were obtained. Similarly, GOS-ACSCs group were obtained though the same process by replacing pure $mSiO_2$ NPs with AHI-encapsulated $mSiO_2$ NPs.

In vitro release: The *in vitro* AHI release behavior was studied using ultra-performance liquid chromatography (UPLC, Agilent 1100, USA) according to a previously reported method [22,93]. Prior to this, the drug concentration in the supernatant after centrifugation of AHI-$mSiO_2$ was measured by HPLC, and the drug encapsulation rate and drug loading rate of AHI-$mSiO_2$ were calculated to be 62.8% and 15.3%, respectively. In brief, samples were immersed in 0.5 mL PBS and shaken at 100 rpm in a shaking incubator. To detect the release kinetics of AHI from GOA, AHI-NPs or GOAS, the total volume of the immersed PBS was obtained after centrifugation. The samples were quickly filtered through a standard sieve, and then 10 μL supernatant was aspirated and measured by UPLC analysis at 367 nm. Finally, the AHI percentage release was calculated against a standard curve.

In vitro composite hydrogel culture: The GOS-ACSCs hydrogel was incubated in chondrogenic induction medium for 7, 14 and 21 days. Then, the samples were collected. The total RNA was isolated from hydrogels using TRIzol reagent (Invitrogen). RIPA lysis buffer (Biocolors, China) was used to obtain total protein content from hydrogels.

Animal surgery procedure: All animal procedures were approved by the Institutional Animal Care and Use Committee of Xin Hua Hospital Affiliated to Shanghai Jiao Tong University School of Medicine. All animals were purchased from Peking University. Adult male New Zealand white rabbits (2.3–2.8 kg) were used for the *in vivo* study. All of the rabbits were raised under the same condition including clean condition, single cage, normal activity, a temperature of 18–23 °C, the relative humidity of 50%–60%, 12 h diurnal rhythm and freedom to eat and drink. The rabbits were randomly divided into three groups: the nontreated group, GOS-ACSCs group and GOAS-ACSCs group. After general anesthetization, rabbits were placed in recumbent position. After making a parapatellar incision, the articular cartilage was exposed by dislocating the patella. A cylindrical cartilage defect (4 mm in diameter, 1.5 mm in depth) was formed in the center of the knee joint trochlear groove using a corneal trephine. A mixture of OSA, GCS, ACSCs and hollow NPs was injected into the cartilage defect site, and hydrogels were formed for 60 s at room temperature in the GOS-ACSCs group. The mixture of OSA, GCS, ACSCs and AHI-NPs was injected into the cartilage defects site, and hydrogels were formed for 1 min at room temperature in the GOAS-ACSCs group. The cartilage defect of the nontreated group was left untreated. Finally, after reduction of the patella, the joint was closed with sutures, and the skin of the knee joint was sutured. The rabbits were injected intramuscularly with penicillin to prevent infection. The rabbits were allowed to move freely in their single cage. After 4, 8, and 12 weeks, rabbits were sacrificed for further study.

Macroscopic evaluation: The repaired tissues were evaluated according to the International Cartilage Repair Society (ICRS) macroscopic score [94]. The scoring of the repaired tissues was carried out by three different investigators.

Histology and immunohistochemistry: Histological specimens were first fixed in 4% paraformaldehyde for 24 h, rinsed with running water for 12 h, and decalcified using 12.5% EDTA for 8 weeks. The decalcified sample was dehydrated by a gradient ethanol series. After the sample was embedded in paraffin, the sample was sagittally cut into sections (5 μm thick) and stained with hematoxylin and eosin (H&E), Safranin O and Fast Green, and toluidine blue. Immunohistochemistry was performed using a standard protocol [95]. Collagen Type II (1:200, #CP18; Calbiochem, Darmstadt, Germany) was used in this study. In brief, sections were digested using pepsin (Sigma-Aldrich, United States) for 30 min at 37 °C for antigen retrieval. 5% goat serum was used to block the sections, and the sections were incubated with the following primary antibodies.

Nanoindentation assessment: Biomechanical testing of regenerated tissues was carried out by previously reported methods of nanoindentation [96,97]. Samples (n = 5) were obtained from knee joints of animals, and used for biomechanical analysis using a TriboIndenter (Hysitron Inc., Minneapolis, MN, USA).

Statistical analysis: The data are presented as the mean ± S.D. as indicated. For the statistical analysis, the differences among groups were calculated by one-way ANOVA after testing for the homogeneity of variance and data from the same group were evaluated by Student's *t-test*. A value of $p < 0.05$ was considered statistically significant.

Declaration of competing interest

We declare that there is no conflict of interests.

CRediT authorship contribution statement

Penglei Cui: Methodology, Investigation, Data curation, Writing – original draft, Visualization, Formal analysis, Funding acquisition. **Panpan Pan:** Methodology, Investigation, Data curation, Writing – original draft, Visualization. **Ling Qin:** Methodology, Investigation, Funding acquisition. **Xinluan Wang:** Methodology, Investigation, Data curation. **Xiaodong Chen:** Investigation, Validation. **Yonghui Deng:** Supervision, Project administration, Funding acquisition, Writing – review & editing. **Xiaoling Zhang:** Conceptualization, Supervision, Project administration, Funding acquisition, Writing – review & editing.

Declaration of competing interest

All authors declared that we have no conflicts of interest to this work.

Acknowledgements

P. L. Cui. and P. P. Pan contributed equally to this work. This work was supported by grants from The Ministry of Science and Technology of China (2020YFC2002800) , the National Natural Science Foundation of China (81830078 , 21875044), NO.2021-NCRC-CXJJ-ZH-35 of Clinical Application-oriented Medical Innovation Foundation from National Clinical Research Center for Orthopedics, Sports Medicine & Rehabilitation and Jiangsu China-Israel Industrial Technical Research Institute Foundation, Sino-Swiss collaborative project from Ministry of Science and Technology (2015DFG32200), Science and Technology Commission of Shanghai Municipality (No.19XD1434100, 19ZR1433100), Shanghai Jiaotong University “Cross research fund of Medical Engineering” (YG2019ZDA22).

Appendix A. Supplementary data

Supplementary data to this article can be found online at https://doi.org/10.1016/j.bioactmat.2022.03.032.

References

[1] Y. Wu, S. Zhu, C. Wu, P. Lu, C. Hu, S. Xiong, J. Chang, B.C. Heng, Y. Xiao, H. W. Ouyang, A Bi-lineage conducive scaffold for osteochondral defect regeneration, Adv. Funct. Mater. 24 (28) (2014) 4473–4483.
[2] O. Behery, R.A. Siston, J.D. Harris, D.C. Flanigan, Treatment of cartilage defects of the knee: expanding on the existing algorithm, Clin. J. Sport Med. 24 (1) (2014) 21–30.
[3] B.J. Huang, J.C. Hu, K.A. Athanasiou, Cell-based tissue engineering strategies used in the clinical repair of articular cartilage, Biomaterials 98 (2016) 1–22.
[4] D.J. Huey, J.C. Hu, K.A. Athanasiou, Unlike bone, cartilage regeneration remains elusive, Science (New York, N.Y.) 338 (6109) (2012) 917–921.
[5] O. Chaudhuri, L. Gu, D. Klumpers, M. Darnell, S.A. Bencherif, J.C. Weaver, N. Huebsch, H.P. Lee, E. Lippens, G.N. Duda, D.J. Mooney, Hydrogels with tunable stress relaxation regulate stem cell fate and activity, Nat. Mater. 15 (3) (2016) 326–334.
[6] F.T. Moutos, L.E. Freed, F. Guilak, A biomimetic three-dimensional woven composite scaffold for functional tissue engineering of cartilage, Nat. Mater. 6 (2) (2007) 162–167.
[7] Y.L. Chen, H.P. Lee, H.Y. Chan, L.Y. Sung, H.C. Chen, Y.C. Hu, Composite chondroitin-6-sulfate/dermatan sulfate/chitosan scaffolds for cartilage tissue engineering, Biomaterials 28 (14) (2007) 2294–2305.
[8] H. Wang, S.C. Heilshorn, Adaptable hydrogel networks with reversible linkages for tissue engineering, Adv. Mater. 27 (25) (2015) 3717–3736.
[9] Y.S. Zhang, A. Khademhosseini, Advances in engineering hydrogels, Science (New York, N.Y.) 356 (6337) (2017).
[10] R. Edri, I. Gal, N. Noor, T. Harel, S. Fleischer, N. Adadi, O. Green, D. Shabat, L. Heller, A. Shapira, I. Gat-Viks, D. Peer, T. Dvir, Personalized hydrogels for engineering diverse fully autologous tissue implants, Adv. Mater. (Deerfield Beach, Fla.) 31 (1) (2019), e1803895.
[11] F. Kai, A.P. Drain, V.M. Weaver, The extracellular matrix modulates the metastatic journey, Dev. Cell 49 (3) (2019) 332–346.
[12] L. Yu, J. Ding, Injectable hydrogels as unique biomedical materials, Chem. Soc. Rev. 37 (8) (2008) 1473–1481.
[13] D.R. Griffin, W.M. Weaver, P.O. Scumpia, D. Di Carlo, T. Segura, Accelerated wound healing by injectable microporous gel scaffolds assembled from annealed building blocks, Nat. Mater. 14 (7) (2015) 737–744.
[14] L. Zhang, J.B. Bailey, R.H. Subramanian, A. Groisman, F.A. Tezcan, Hyperexpandable, self-healing macromolecular crystals with integrated polymer networks, Nature 557 (7703) (2018) 86–91.
[15] H. Yuk, T. Zhang, G.A. Parada, X. Liu, X. Zhao, Skin-inspired hydrogel-elastomer hybrids with robust interfaces and functional microstructures, Nat. Commun. 7 (2016) 12028.
[16] T.E. Brown, K.S. Anseth, Spatiotemporal hydrogel biomaterials for regenerative medicine, Chem. Soc. Rev. 46 (21) (2017) 6532–6552.
[17] L. Han, L. Yan, K. Wang, L. Fang, H. Zhang, Y. Tang, Y. Ding, L.-T. Weng, J. Xu, J. Weng, Y. Liu, F. Ren, X. Lu, Tough, self-healable and tissue-adhesive hydrogel with tunable multifunctionality, NPG Asia Mater. 9 (4) (2017) e372-e372.
[18] S. Tang, B.M. Richardson, K.S. Anseth, Dynamic covalent hydrogels as biomaterials to mimic the viscoelasticity of soft tissues, Prog. Mater. Sci. 120 (2021).
[19] M.C. Wan, W. Qin, C. Lei, Q.H. Li, M. Meng, M. Fang, W. Song, J.H. Chen, F. Tay, L. N. Niu, Biomaterials from the sea: future building blocks for biomedical applications, Bioact. Mater. 6 (12) (2021) 4255–4285.
[20] M. Zhang, X. Qiao, W. Han, T. Jiang, F. Liu, X. Zhao, Alginate-chitosan oligosaccharide-ZnO composite hydrogel for accelerating wound healing, Carbohydr. Polym. 266 (2021) 118100.
[21] P. Pan, X. Chen, H. Xing, Y. Deng, J. Chen, F.A. Alharthi, A.A. Alghamdi, J. Su, A fast on-demand preparation of injectable self-healing nanocomposite hydrogels for efficient osteoinduction, Chin. Chem. Lett. 32 (7) (2021) 2159–2163.
[22] D. Shi, X. Xu, Y. Ye, K. Song, Y. Cheng, J. Di, Q. Hu, J. Li, H. Ju, Q. Jiang, Z. Gu, Photo-cross-linked scaffold with Kartogenin-encapsulated nanoparticles for cartilage regeneration, ACS Nano 10 (1) (2016) 1292–1299.
[23] Y. Weng, J. Liu, S. Jin, W. Guo, X. Liang, Z. Hu, Nanotechnology-based strategies for treatment of ocular disease, Acta Pharm. Sin. B 7 (3) (2017) 281–291.
[24] J. Meng, J. Xing, X. Ma, W. Cao, J. Lu, Y. Wang, X. Gao, B. Sun, X. Liang, Y. Zhao, Metallofullerol nanoparticles with low toxicity inhibit tumor growth by induction of G0/G1 arrest, Nanomedicine (London, England) 8 (2) (2013) 203–213.
[25] J. Meng, J. Xing, Y. Wang, J. Lu, Y. Zhao, X. Gao, P.C. Wang, L. Jia, X. Liang, Epigenetic modulation of human breast cancer by metallofullerenol nanoparticles: in vivo treatment and in vitro analysis, Nanoscale 3 (11) (2011) 4713–4719.
[26] J. Liu, G. Yang, W. Zhu, Z. Dong, Y. Yang, Y. Chao, Z. Liu, Light-controlled drug release from singlet-oxygen sensitive nanoscale coordination polymers enabling cancer combination therapy, Biomaterials 146 (2017) 40–48.
[27] H. Wang, Y. Chao, J. Liu, W. Zhu, G. Wang, L. Xu, Z. Liu, Photosensitizer-crosslinked in-situ polymerization on catalase for tumor hypoxia modulation & enhanced photodynamic therapy, Biomaterials 181 (2018) 310–317.
[28] Y. Wen, Y. Wang, X. Liu, W. Zhang, X. Xiong, Z. Han, X. Liang, Camptothecin-based nanodrug delivery systems, Cancer Biol. Med. 14 (4) (2017) 363–370.
[29] P. Pan, Q. Yue, J. Li, M. Gao, X. Yang, Y. Ren, X. Cheng, P. Cui, Y. Deng, Smart cargo delivery system based on mesoporous nanoparticles for bone disease diagnosis and treatment, Adv. Sci. (2021), 2004586.
[30] Y. Zou, B. Huang, L. Cao, Y. Deng, J. Su, Tailored mesoporous inorganic biomaterials: assembly, functionalization, and drug delivery engineering, Adv. Mater. 33 (2) (2021), e2005215.
[31] M. Diba, W.A. Camargo, M. Brindisi, K. Farbod, A. Klymov, S. Schmidt, M. J. Harrington, L. Draghi, A.R. Boccaccini, J.A. Jansen, J.J.J.P. van den Beucken, S. C.G. Leeuwenburgh, Composite colloidal gels made of bisphosphonate-functionalized gelatin and bioactive glass particles for regeneration of osteoporotic bone defects, Adv. Funct. Mater. 27 (45) (2017).
[32] R.K. Kankala, Y.H. Han, J. Na, C.H. Lee, Z. Sun, S.B. Wang, T. Kimura, Y.S. Ok, Y. Yamauchi, A.Z. Chen, K.C. Wu, Nanoarchitectured structure and surface biofunctionality of mesoporous silica nanoparticles, Adv. Mater. 32 (23) (2020), e1907035.
[33] Z. Li, Z. Liu, M. Yin, X. Yang, Q. Yuan, J. Ren, X. Qu, Aptamer-capped multifunctional mesoporous strontium hydroxyapatite nanovehicle for cancer-cell-responsive drug delivery and imaging, Biomacromolecules 13 (12) (2012) 4257–4263.
[34] J. Liu, B. Cai, L. Cui, C.-L. Chen, Peptoid-based hierarchically-structured biomimetic nanomaterials: synthesis, characterization and applications, Sci. China Mater. 63 (7) (2020) 1099–1112.
[35] X. Xue, Y. Hu, Y. Deng, J. Su, Recent advances in design of functional biocompatible hydrogels for bone tissue engineering, Adv. Funct. Mater. 31 (19) (2021).
[36] X. Wang, O. Ronsin, B. Gravez, N. Farman, T. Baumberger, F. Jaisser, T. Coradin, C. Helary, Nanostructured dense collagen-polyester composite hydrogels as amphiphilic platforms for drug delivery, Adv Sci (Weinh) 8 (7) (2021) 2004213.
[37] P. Pan, Q. Yue, J. Li, M. Gao, X. Yang, Y. Ren, X. Cheng, P. Cui, Y. Deng, Smart cargo delivery system based on mesoporous nanoparticles for bone disease diagnosis and treatment, Adv. Sci. 8 (12) (2021), e2004586.
[38] P. Mora-Raimundo, D. Lozano, M. Benito, F. Mulero, M. Manzano, M. Vallet-Regi, Osteoporosis remission and new bone formation with mesoporous silica nanoparticles, Adv Sci (Weinh) 8 (16) (2021), e2101107.
[39] W.-H. Chen, W.-C. Liao, Y.S. Sohn, M. Fadeev, A. Cecconello, R. Nechushtai, I. Willner, Stimuli-Responsive nucleic acid-based polyacrylamide hydrogel-coated metal-organic framework nanoparticles for controlled drug release, Adv. Funct. Mater. 28 (8) (2018).
[40] X. Wang, O. Ronsin, B. Gravez, N. Farman, T. Baumberger, F. Jaisser, T. Coradin, C. Hélary, Nanostructured dense collagen-polyester composite hydrogels as amphiphilic platforms for drug delivery, Adv. Sci. 8 (7) (2021), 2004213.
[41] J. Cheng, D. Amin, J. Latona, E. Heber-Katz, P.B. Messersmith, Supramolecular polymer hydrogels for drug-induced tissue regeneration, ACS Nano 13 (5) (2019) 5493–5501.
[42] J. Tan, M. Zhang, Z. Hai, C. Wu, J. Lin, W. Kuang, H. Tang, Y. Huang, X. Chen, G. Liang, Sustained release of two bioactive factors from supramolecular hydrogel promotes periodontal bone regeneration, ACS Nano 13 (5) (2019) 5616–5622.
[43] P.M. Gilbert, K.L. Havenstrite, K.E. Magnusson, A. Sacco, N.A. Leonardi, P. Kraft, N.K. Nguyen, S. Thrun, M.P. Lutolf, H.M. Blau, Substrate elasticity regulates skeletal muscle stem cell self-renewal in culture, Science (New York, N.Y.) 329 (5995) (2010) 1078–1081.
[44] Y. Lee, S.H. Cha, Y.W. Kim, D. Choi, J.Y. Sun, Transparent and attachable ionic communicators based on self-cleanable triboelectric nanogenerators, Nat. Commun. 9 (1) (2018) 1804.
[45] F. Yang, J. Zhao, W.J. Koshut, J. Watt, J.C. Riboh, K. Gall, B.J. Wiley, A synthetic hydrogel composite with the mechanical behavior and durability of cartilage, Adv. Funct. Mater. 30 (36) (2020), 2003451.
[46] P. Thoniyot, M.J. Tan, A.A. Karim, D.J. Young, X.J. Loh, Nanoparticle-hydrogel composites: concept, design, and applications of these promising, multi-functional materials, Adv Sci (Weinh) 2 (1–2) (2015) 1400010.

[47] E.A. Appel, M.W. Tibbitt, M.J. Webber, B.A. Mattix, O. Veiseh, R. Langer, Self-assembled hydrogels utilizing polymer-nanoparticle interactions, Nat. Commun. 6 (2015) 6295.

[48] M. Liu, Y. Ishida, Y. Ebina, T. Sasaki, T. Hikima, M. Takata, T. Aida, An anisotropic hydrogel with electrostatic repulsion between cofacially aligned nanosheets, Nature 517 (7532) (2015) 68–72.

[49] H. Qin, T. Zhang, N. Li, H.P. Cong, S.H. Yu, Anisotropic and self-healing hydrogels with multi-responsive actuating capability, Nat. Commun. 10 (1) (2019) 2202.

[50] H. Cho, J. Kim, S. Kim, Y.C. Jung, Y. Wang, B.J. Kang, K. Kim, Dual delivery of stem cells and insulin-like growth factor-1 in coacervate-embedded composite hydrogels for enhanced cartilage regeneration in osteochondral defects, J. Contr. Release 327 (2020) 284–295.

[51] C. Qi, J. Liu, Y. Jin, L. Xu, G. Wang, Z. Wang, L. Wang, Photo-crosslinkable, injectable sericin hydrogel as 3D biomimetic extracellular matrix for minimally invasive repairing cartilage, Biomaterials 163 (2018) 89–104.

[52] M. Liu, X. Zeng, C. Ma, H. Yi, Z. Ali, X. Mou, S. Li, Y. Deng, N. He, Injectable hydrogels for cartilage and bone tissue engineering, Bone Res. 5 (2017) 17014.

[53] K. Ren, C. He, C. Xiao, G. Li, X. Chen, Injectable glycopolypeptide hydrogels as biomimetic scaffolds for cartilage tissue engineering, Biomaterials 51 (2015) 238–249.

[54] F. Zhou, Y. Hong, X. Zhang, L. Yang, J. Li, D. Jiang, V. Bunpetch, Y. Hu, H. Ouyang, S. Zhang, Tough hydrogel with enhanced tissue integration and in situ forming capability for osteochondral defect repair, Appl. Mater. Today 13 (2018) 32–44.

[55] G. Chu, C. Shi, H. Wang, W. Zhang, H. Yang, B. Li, Strategies for annulus fibrosus regeneration: from biological therapies to tissue engineering, Front. Bioeng. Biotechnol. 6 (2018) 90–113.

[56] M. Gao, W. Gao, J.M. Papadimitriou, C. Zhang, J. Gao, M. Zheng, Exosomes-the enigmatic regulators of bone homeostasis, Bone Res. 6 (2018) 36–49.

[57] A.M. Kloxin, A.M. Kasko, C.N. Salinas, K.S. Anseth, Photodegradable hydrogels for dynamic tuning of physical and chemical properties, Science (New York, N.Y.) 324 (5923) (2009) 59–63.

[58] T. Kurth, E. Hedbom, N. Shintani, M. Sugimoto, F.H. Chen, M. Haspl, S. Martinovic, E.B. Hunziker, Chondrogenic potential of human synovial mesenchymal stem cells in alginate, Osteoarthritis Cartilage 15 (10) (2007) 1178–1189.

[59] M.F. Pittenger, A.M. Mackay, S.C. Beck, R.K. Jaiswal, R. Douglas, J.D. Mosca, M. A. Moorman, D.W. Simonetti, S. Craig, D.R. Marshak, Multilineage potential of adult human mesenchymal stem cells, Science (New York, N.Y.) 284 (5411) (1999) 143–147.

[60] K.H. Choi, B.H. Choi, S.R. Park, B.J. Kim, B.H. Min, The chondrogenic differentiation of mesenchymal stem cells on an extracellular matrix scaffold derived from porcine chondrocytes, Biomaterials 31 (20) (2010) 5355–5365.

[61] J.H. Cui, K. Park, S.R. Park, B.H. Min, Effects of low-intensity ultrasound on chondrogenic differentiation of mesenchymal stem cells embedded in polyglycolic acid: an in vivo study, Tissue Eng. 12 (1) (2006) 75–82.

[62] K. Pelttari, A. Winter, E. Steck, K. Goetzke, T. Hennig, B.G. Ochs, T. Aigner, W. Richter, Premature induction of hypertrophy during in vitro chondrogenesis of human mesenchymal stem cells correlates with calcification and vascular invasion after ectopic transplantation in SCID mice, Arthritis Rheum. 54 (10) (2006) 3254–3266.

[63] E.A. Aisenbrey, S.J. Bryant, The role of chondroitin sulfate in regulating hypertrophy during MSC chondrogenesis in a cartilage mimetic hydrogel under dynamic loading, Biomaterials 190–191 (2019) 51–62.

[64] Y. Jiang, R.S. Tuan, Origin and function of cartilage stem/progenitor cells in osteoarthritis, Nat. Rev. Rheumatol. 11 (4) (2015) 206–212.

[65] W. Tong, Y. Geng, Y. Huang, Y. Shi, S. Xiang, N. Zhang, L. Qin, Q. Shi, Q. Chen, K. Dai, X. Zhang, In vivo identification and induction of articular cartilage stem cells by inhibiting NF-κB signaling in osteoarthritis, Stem Cell. 33 (10) (2015) 3125–3137.

[66] S. Fickert, J. Fiedler, R.E. Brenner, Identification of subpopulations with characteristics of mesenchymal progenitor cells from human osteoarthritic cartilage using triple staining for cell surface markers, Arthritis Res. Ther. 6 (5) (2004) R422–R432.

[67] R. Williams, I.M. Khan, K. Richardson, L. Nelson, H.E. McCarthy, T. Analbelsi, S. K. Singhrao, G.P. Dowthwaite, R.E. Jones, D.M. Baird, H. Lewis, S. Roberts, H. M. Shaw, J. Dudhia, J. Fairclough, T. Briggs, C.W. Archer, Identification and clonal characterisation of a progenitor cell sub-population in normal human articular cartilage, PLoS One 5 (10) (2010), e13246.

[68] A. Quintin, C. Schizas, C. Scaletta, S. Jaccoud, L.A. Applegate, D.P. Pioletti, Plasticity of fetal cartilaginous cells, Cell Transplant. 19 (10) (2010) 1349–1357.

[69] C. Karlsson, A. Lindahl, Articular cartilage stem cell signalling, Arthritis Res. Ther. 11 (4) (2009) 121.

[70] S. Hattori, C. Oxford, A.H. Reddi, Identification of superficial zone articular chondrocyte stem/progenitor cells, Biochem. Biophys. Res. Commun. 358 (1) (2007) 99–103.

[71] A.J. Hayes, D. Tudor, M.A. Nowell, B. Caterson, C.E. Hughes, Chondroitin sulfate sulfation motifs as putative biomarkers for isolation of articular cartilage progenitor cells, J. Histochem. Cytochem. 56 (2) (2008) 125–138.

[72] A.S. Brack, T.A. Rando, Tissue-specific stem cells: lessons from the skeletal muscle satellite cell, Cell Stem Cell 10 (5) (2012) 504–514.

[73] E. Kozhemyakina, M. Zhang, A. Ionescu, U.M. Ayturk, N. Ono, A. Kobayashi, H. Kronenberg, M.L. Warman, A.B. Lassar, Identification of a Prg4-Expressing Articular Cartilage Progenitor Cell Population in Mice, 67, 2015, pp. 1261–1273, 5.

[74] I.M. Khan, L. Francis, P.S. Theobald, S. Perni, R.D. Young, P. Prokopovich, R. S. Conlan, C.W. Archer, In vitro growth factor-induced bio engineering of mature articular cartilage, Biomaterials 34 (5) (2013) 1478–1487.

[75] A.L. Harvey, R. Edrada-Ebel, R.J. Quinn, The re-emergence of natural products for drug discovery in the genomics era, Nat. Rev. Drug Discov. 14 (2) (2015) 111–129.

[76] D.J. Newman, G.M. Cragg, Natural products as sources of new drugs from 1981 to 2014, J. Nat. Prod. 79 (3) (2016) 629–661.

[77] J.L. Geng, Y. Dai, Z.H. Yao, Z.F. Qin, X.L. Wang, L. Qin, X.S. Yao, Metabolites profile of Xian-Ling-Gu-Bao capsule, a traditional Chinese medicine prescription, in rats by ultra performance liquid chromatography coupled with quadrupole time-of-flight tandem mass spectrometry analysis, J. Pharm. Biomed. Anal. 96 (2014) 90–103.

[78] H. Wu, Q. Zhong, J. Wang, M. Wang, F. Fang, Z. Xia, R. Zhong, H. Huang, Z. Ke, Y. Wei, L. Feng, Z. Shi, E. Sun, J. Song, X. Jia, Beneficial effects and toxicity studies of Xian-ling-gu-bao on bone metabolism in ovariectomized rats, Front. Pharmacol. 8 (2017) 273.

[79] Z.-G. Zheng, Y.-P. Zhou, X. Zhang, P.M. Thu, Z.-S. Xie, C. Lu, T. Pang, B. Xue, D.-Q. Xu, Y. Chen, X.-W. Chen, H.-J. Li, X. Xu, Anhydroicaritin improves diet-induced obesity and hyperlipidemia and alleviates insulin resistance by suppressing SREBPs activation, Biochem. Pharmacol. 122 (2016) 42–61.

[80] Z.-G. Zheng, X. Zhang, Y.-P. Zhou, C. Lu, P.M. Thu, C. Qian, M. Zhang, P. Li, H.-J. Li, X. Xu, Anhydroicaritin, a SREBPs inhibitor, inhibits RANKL-induced osteoclastic differentiation and improves diabetic osteoporosis in STZ-induced mice, Eur. J. Pharmacol. 809 (2017) 156–162.

[81] T.C. Tseng, L. Tao, F.Y. Hsieh, Y. Wei, I.M. Chiu, S.H. Hsu, An injectable, self-healing hydrogel to repair the central nervous system, Adv. Mater. 27 (23) (2015) 3518–3524.

[82] C. Gao, M. Liu, J. Chen, X. Zhang, Preparation and controlled degradation of oxidized sodium alginate hydrogel, Polym. Degrad. Stabil. 94 (9) (2009) 1405–1410.

[83] H. Zhang, S. Syed, C.F. Barbas 3rd, Highly enantio- and diastereoselective Mannich reactions of glycine Schiff bases with in situ generated N-Boc-imines catalyzed by a cinchona alkaloid thiourea, Org. Lett. 12 (4) (2010) 708–711.

[84] B. Yang, Y. Zhang, X. Zhang, L. Tao, S. Li, Y. Wei, Facilely prepared inexpensive and biocompatible self-healing hydrogel: a new injectable cell therapy carrier, Polym. Chem. 3 (12) (2012).

[85] Y. Jiang, C. Lee, Q. Wang, Y. Deng, D. Fu, Monodisperse mesoporous silica nanospheres with radially oriented mesochannels and their size effect on cell uptake, Microporous Mesoporous Mater. 181 (2013) 248–253.

[86] S. Zhang, S.J. Chuah, R.C. Lai, J.H.P. Hui, S.K. Lim, W.S. Toh, MSC exosomes mediate cartilage repair by enhancing proliferation, attenuating apoptosis and modulating immune reactivity, Biomaterials 156 (2018) 16–27.

[87] M. Borne, N. Raijmakers, J. Vanlauwe, J. Victor, S. Jong, J. Bellemans, D. Saris, International cartilage repair society (ICRS) and oswestry macroscopic cartilage evaluation scores validated for use in autologous chondrocyte implantation (ACI) and microfracture, Osteoarthritis Cartilage 15 (12) (2007) 1397–1402.

[88] Y. Liu, L. Peng, L. Li, C. Huang, K. Shi, X. Meng, P. Wang, M. Wu, L. Li, H. Cao, K. Wu, Q. Zeng, H. Pan, W.W. Lu, L. Qin, C. Ruan, X. Wang, 3D-bioprinted BMSC-laden biomimetic multiphasic scaffolds for efficient repair of osteochondral defects in an osteoarthritic rat model, Biomaterials 279 (2021) 121216.

[89] L. Zhang, X. Zhang, K.F. Li, D.X. Li, Y.M. Xiao, Y.J. Fan, X.D. Zhang, Icariin promotes extracellular matrix synthesis and gene expression of chondrocytes in vitro, Phytother Res. 26 (9) (2012) 1385–1392.

[90] W. Shi, M. Sun, X. Hu, B. Ren, J. Cheng, C. Li, X. Duan, X. Fu, J. Zhang, H. Chen, Y. Ao, Structurally and functionally optimized silk-fibroin-gelatin scaffold using 3D printing to repair cartilage injury in vitro and in vivo, Adv. Mater. 29 (29) (2017).

[91] X. Wang, Y. Zhang, W. Luo, A.A. Elzatahry, X. Cheng, A. Alghamdi, A.M. Abdullah, Y. Deng, D. Zhao, Synthesis of ordered mesoporous silica with tunable morphologies and pore sizes via a nonpolar solvent-assisted stöber method, Chem. Mater. 28 (7) (2016) 2356–2362.

[92] C.G. Gomez, M. Rinaudo, M.A. Villar, Oxidation of sodium alginate and characterization of the oxidized derivatives, Carbohydr. Polym. 67 (3) (2007) 296–304.

[93] P. Pan, J. Chen, T. Fan, Y. Hu, T. Wu, Q. Zhang, Facile preparation of biphasic-induced magnetic icariin-loaded composite microcapsules by automated in situ click technology, Colloids Surf. B Biointerfaces 140 (2016) 50–59.

[94] M.P. van den Borne, N.J. Raijmakers, J. Vanlauwe, J. Victor, S.N. de Jong, J. Bellemans, D.B. Saris, International cartilage repair society (ICRS) and oswestry macroscopic cartilage evaluation scores validated for use in autologous chondrocyte implantation (ACI) and microfracture, Osteoarthritis Cartilage 15 (12) (2007) 1397–1402.

[95] A.M. Altman, Y. Yan, N. Matthias, X. Bai, C. Rios, A.B. Mathur, Y.H. Song, E.U. Alt, IFATS collection: human adipose-derived stem cells seeded on a silk fibroin-chitosan scaffold enhance wound repair in a murine soft tissue injury model, Stem Cell. 27 (1) (2009) 250–258.

[96] C. Li, L.A. Pruitt, K.B. King, Nanoindentation differentiates tissue-scale functional properties of native articular cartilage, J. Biomed. Mater. Res. 78 (4) (2006) 729–738.

[97] O. Franke, K. Durst, V. Maier, M. Göken, T. Birkholz, H. Schneider, F. Hennig, K. Gelse, Mechanical properties of hyaline and repair cartilage studied by nanoindentation, Acta Biomater. 3 (6) (2007) 873–881.